Effects of SiO_2 and Al_2O_3 Nanofillers on Polyethylene Properties

Denis Panaitescu,[1] Florin Ciuprina,[2] Michaela Iorga,[1] Adriana Frone,[1] Constantin Radovici,[1] Marius Ghiurea,[1] Serban Sever,[1] Ilona Plesa[2]

[1]*Polymer Department, National Institute of Research and Development in Chemistry and Petrochemistry ICECHIM, 202 Spl. Independentei, Bucharest 060021, Romania*
[2]*ELMAT Laboratory, Faculty of Electrical Engineering, POLITEHNICA University of Bucharest, 313 Splaiul Independentei, Bucharest 060042, Romania*

Received 7 October 2009; accepted 6 February 2011
DOI 10.1002/app.34297
Published online 10 June 2011 in Wiley Online Library (wileyonlinelibrary.com).

ABSTRACT: Polymers filled with inorganic nanoparticles have become interesting materials as dielectrics because of their improved mechanical and electrical properties compared with the unfilled polymers and with polymer microcomposites. These improvements are mainly due to the large surface area of nanoparticles and new polymer–nanofiller interface characteristics. In the present work, polyethylene nanocomposites with SiO_2 and Al_2O_3 nanoparticles were prepared by melt mixing. Mechanical and electrical properties of these composites were determined and morphological aspects were revealed by scanning electron microscopy, wide-angle X-ray diffraction, and atomic force microscopy. The effect of nanostructure and the importance of nanofiller dispersion were analyzed in connection with mechanical and electrical properties. J Appl Polym Sci 122: 1921–1935, 2011

Key words: nanocomposites; mechanical properties; dielectric properties; polyethylene (PE); atomic force microscopy (AFM)

INTRODUCTION

In the last decades, polymer nanocomposites have become a very attractive alternative to conventional filled polymers. Many recent studies revealed an improvement of mechanical, electrical, chemical, or thermal properties in some of these promising polymer-nanofiller systems with respect to traditional polymer composites having micron-sized fillers.[1–6]

The polymer nanocomposites properties depend on many factors including the type of the polymer and of the nanofiller, the interface properties, the preparation method, and so forth.[2,4–10] Polyolefins are semicrystalline polymers, widely used due to their good balance of physical and chemical properties, low cost, and ease of processing. Polyolefin nanocomposites with different nanofillers including clay,[8–13] carbon nanotubes,[14,15] carbon nanofibers (CNFs),[16] silica,[14,17–20] calcium carbonate,[21] polyhedral oligomeric silsequioxanes,[22] were prepared by melt compounding to enhance various properties. Thus, an improvement of the thermal stability and of gas barrier properties were obtained for high density polyethylene (HDPE) nanocomposites containing 2.5 wt % of carbon nanotubes, montmorillonite or silica nanoparticles, an increase in the elastic modulus and a decrease of tensile and impact strength being also signaled.[14] The tensile strength and modulus of ultra high molecular weight polyethylene/low density polyethylene (LDPE) blends have been increased by the addition of CNFs that also determined a nonlinear decrease in the degree of crystallinity of polymer nanocomposites.[16] When silica nanoparticles were introduced into a LDPE-EVA blend, both the crystalline structure and the degree of crystallinity were affected: the degree of crystallinity decreased, crystalline size increased, and interplanar distances did not change. An appreciable improvement of tensile properties was detected only in the case of silane-treated nanosilica containing LDPE-EVA nanocomposites.[18]

A good dispersion of hydrophilic nanofillers in polyethylene is difficult to be obtained because of the strong hydrophobicity of the matrix. This drawback is usually overcomed by the surface modification of nanofillers or by using adhesion-promoting agents.[10,12,23] The latter method is easier to apply and maleic anhydride-modified polyolefins have proven to be effective compatibilizing agents.[10,23] Some studies have emphasized the effect of interfacial interactions and nanosilica dispersion on the mechanical properties of polyolefin-based nanocomposites prepared by melt compounding. Rong et al.

Correspondence to: D. Panaitescu (panaitescu@icf.ro).
Contract grant sponsor: Romanian National Authority for Scientific Research.

have applied different treatments to overcome nanoparticles agglomeration and to obtain different interfacial interactions in case of polypropylene (PP)/silica nanocomposites prepared by melt mixing PP powder with 10-nm surface treated silica particles in a Brabender Plasticorder.[17] The strongest interaction and the best values for yield stress were obtained in the case of low silica concentration and low percentage of grafting. However, the modulus of elasticity of nanocomposites containing grafted silica was lower than that of nanocomposites with untreated silica.[17] Zhang et al.[20] obtained similar values of the modulus of elasticity for both treated and untreated silica containing nanocomposites using HDPE instead of PP as a matrix, but the same pretreatment of silica particles and manufacturing procedure. They considered the specific viscoelastic feature of the interphase and the matching of components properties as key issues of tailoring composite performances.[20]

Insulation integrity is of great importance for all-electrical power applications, including energy conversion, power delivery, energy storage, and power consumption. Polymer nanocomposites with dielectric and insulating properties, also known as nanodielectrics could be in the near future one of the most preferred solutions for developing more reliable and application tailored electrical insulating systems. This is supported by the continuously increasing evidences about the improvement of the dielectric behavior of the nanodielectrics compared to unfilled polymers and to polymer microcomposites.[24–27] For example, nano-TiO_2 filled polyethylene and epoxy composites have shown an increase in dielectric strength and a reduction in space charge compared to micron size TiO_2 filled polyethylene and epoxy, respectively.[25,26]

Dielectric properties as well as mechanical properties of polymer nanocomposites are strongly influenced by the huge nanofiller–polymer interface, by the nanofiller dispersion in the polymer matrix and by thermal treatments.[28–34] For instance, LDPE/ZnO (200 nm) composites prepared by melt compounding were thermal treated by annealing (50°C for 50 h) and quenching (rapidly dropping of molten samples in ice water). An increase in the dielectric constant of LDPE/ZnO nanocomposites with ZnO content was observed for all samples, regardless of the thermal treatment applied, but the dielectric constant of annealed LDPE/ZnO nanocomposites was higher than that of quenched samples.[34] Tjong et al. explained this behavior by morphological changes owing to these treatments—for example, annealed nanocomposites exhibit higher degree of crystallinity than quenched samples having more perfect crystals, thus allowing ZnO clusters formation.[34] Despite the encouraging advances in the field of polymer nanocomposites, understanding and controlling the relationship between the properties (electrical, mechanical, etc.) and the nanostructure are far from being completely solved problems.

In this contribution, preliminary results concerning the investigation of mechanical and electrical properties of polyethylene nanocomposites with inorganic fillers in relation with the nanodispersion of the fillers and polymer morphology are presented. Two types of nanofillers, silicon dioxide (SiO_2) and aluminum oxide (Al_2O_3) were used to prepare the samples of polyethylene nanocomposites studied in this work. These nanofillers were chosen for generating different level of dielectric characteristics and different interfacial interactions.

To improve the compatibility of nanofillers with polyethylene, a maleic anhydride graft polyethylene was used. Mechanical, electrical, and thermal properties of these composites were explored and discussed in correlation with morphological aspects revealed by scanning electron microscopy (SEM), X-ray diffraction and, especially, by atomic force microscopy (AFM), which is a powerful technique for compositional imaging of polymer nanocomposites and provides detailed information regarding the surface morphology of samples.[35]

EXPERIMENTAL

Materials and analytical instruments

A LDPE with a melt flow index (190°C, 2.16 kg) of 0.3 g/10 min and a tensile strength of 14.0 MPa, supplied by Arpechim, Romania, was used as polymer matrix. A maleic anhydride grafted polyethylene (MA-PE) from Aldrich Co., with a density of 0.925 g/cm^3, a melting point of 105°C, and containing 3 wt % grafted maleic anhydride was used as a compatibilizing agent. The fillers—silica nanopowder, with a content of 99.5% SiO_2, the average particle diameter of 15 nm, density 2.2 g/cm^3, bulk density 0.011 g/cm^3, and the specific surface area of 180 m^2/g, and aluminum oxide nanopowder, with the average particle diameter of 45 nm, density 3.5 g/cm^3, and the specific surface area of 40 m^2/g—were supplied by Sigma-Aldrich Co. (Saint Louis, Missouri) as well.

A Brabender Plasticorder LabStation was used for mixing and homogenizing each nanopowder type (concentration of 1, 2, 5, or 10 wt %) with the polymer matrix and the compatibilizing agent (5 wt %) at a temperature of 160–165°C and having the speed of the rotors of 75 rpm. Nanopowders were added slowly in the polymer melt over a period of 10 min. When all the materials were added into the mixing chamber, the materials were mixed for another 10 min. These mixing conditions were chosen after

microscopic investigation of PE/5% nano-oxides films, obtained in different mixing conditions. The samples used for the measurements, square plates 150 × 150 × 2 mm for mechanical characterization and 100 × 100 × 0.5 mm for electrical tests, wide-angle X-ray diffraction (WAXD) and microscopic characterization, were prepared by hot pressing in an electrically heated press at 170°C for 5 min with a force of 50 kN. After compression molding, the samples were cooled to room temperature under pressure for another 30 min. The optimum mechanical properties were obtained for this cooling rate. The sample containing polyethylene and 5% MA-PE was designated as a reference. Since all samples contain MA-PE, inclusive of the reference, this will be omitted from the name of the samples.

A Quanta Scanning Electron Microscope 200 served for microscopic investigations of nanocomposites (accelerating voltage 10 kV, no coating) and A DRON-2.0 X-ray Diffractometer (horizontal goniometer–Bragg-Brentano geometry–reflexion) using CuK $\overline{\alpha}$ radiation with $\lambda = 1.5406$ Å was used for morphological investigation.

AFM images were captured in ScanAsyst mode by a MultiMode 8 atomic force microscope equipped with a Nanoscope V converter (Bruker Nano Division, Santa Barbara, California). ScanAsyst mode automatically optimizes imaging parameters including set-point, feedback gains, and scan rate to get an optimized image. It utilizes peak force tapping mode that performs a very fast force curve at every pixel in the image, the peak force of these curves being used as the imaging feedback signal, which allows direct control of imaging force. Real time scanning was performed in air at room temperature with scan rates of 0.8 Hz and scan angle 0°. A silicon tip (nominal radius 2 nm, from Bruker) with a cantilever length of 115 μm and a resonant frequency of about 70 kHz was used. The images (256 × 256) were recorded and analyzed using the AFM software NanoScope version 1.20.

Thermal analysis was performed using a Dupont TA 2100 differential scanning calorimeter in the temperature range 40–180°C at a heating rate of 10°C/min and using alumina crucibles. Measurements were carried out using 10–12 mg of each sample, with an empty crucible as the reference. Temperature and enthalpy calibration were made with a standard sample of indium, using its melting transition (156.61°C, 3296 kJ/mol). An overall accuracy of ± 0.5°C in temperature and ± 1% in enthalpy is estimated.

Tensile properties of the composites were determined according to ISO 527 on specimens type IB (five specimens for each test) with 50 mm/min for the tensile strength and 2 mm/min for the modulus of elasticity, using an Instron 3382 Universal Testing Machine. According to ISO 527, the modulus of elasticity was determined from the slope of stress–strain curves between two strain values: 0.0005 and 0.0025 mm/mm, using the software of the Instron 3382, Bluehill 2 device. It is considered that the creep does not affect modulus values because it has been determined at low enough values of strain, and hence, of the force, according ISO 527, providing values of force that did not involve the creep component build-up.

The real part of the permittivity (ε_r') and the loss tangent (tan δ) were determined by dielectric spectroscopy using a Novocontrol ALPHA-A Analyzer in combination with an Active Sample Cell ZGS, over the frequency range 10^{-3} to 10^6 Hz, at ambient temperature (25°C).

RESULTS AND DISCUSSION

Microscopic investigation

The dispersion of nanoparticles in polyethylene has been first investigated by SEM on pressed plates of PE/5 wt % nano-oxides samples. The dispersion of SiO_2 nanoparticles in the polyethylene matrix, after melt processing, is observed in Figure 1(a). In the uppermost polymer surface layer, SiO_2 nanoparticles are detected as small aggregates of different forms, containing 5–10 nanoparticles, but single or small groups of 2–3 particles are also observed, indicating a satisfying dispersion of SiO_2 nanoparticles in the matrix. The SEM image of PE/5 wt % Al_2O_3 sample [Fig. 1(b)] shows single Al_2O_3 nanoparticles and small groups of 2–3 nanoparticles in the nanometric surface layer of the sample. Al_2O_3 nanoparticles (45 nm) are easily observed in the microscopic image because of their larger diameter relative to SiO_2 nanoparticles (15 nm), and their uniform distribution can also be noticed. Compared to nanocomposite samples, SEM image of PE [Fig. 1(c)] shows only some superficial impurities and broken gas bubbles.

A nanolevel dispersion of silica and alumina particles in polyethylene seems to appear in SEM images. The dispersion level of nanofillers in the matrix and the morphology of nanocomposites have a huge influence on some macroscopic characteristics of polyethylene nanocomposites. To clarify the peculiarities of surface morphology of different samples, AFM images were obtained on thin pressed plates of PE, PE containing MA-PE, and PE/5 wt % nano-oxides samples. The 2D and 3D height images of PE [Fig. 2(a)] show an ordered pattern with ribbon-like structures separated by less-ordered domains. The linear structures could be assigned to the edges of the lamellae and the bright bands to the lamellae. The size of these domains is between 50 and 80 nm, a similar structural organization being found in the case of LDPE composite containing nano-TiO_2 particles.[36] Unlike PE, the reference (which contains

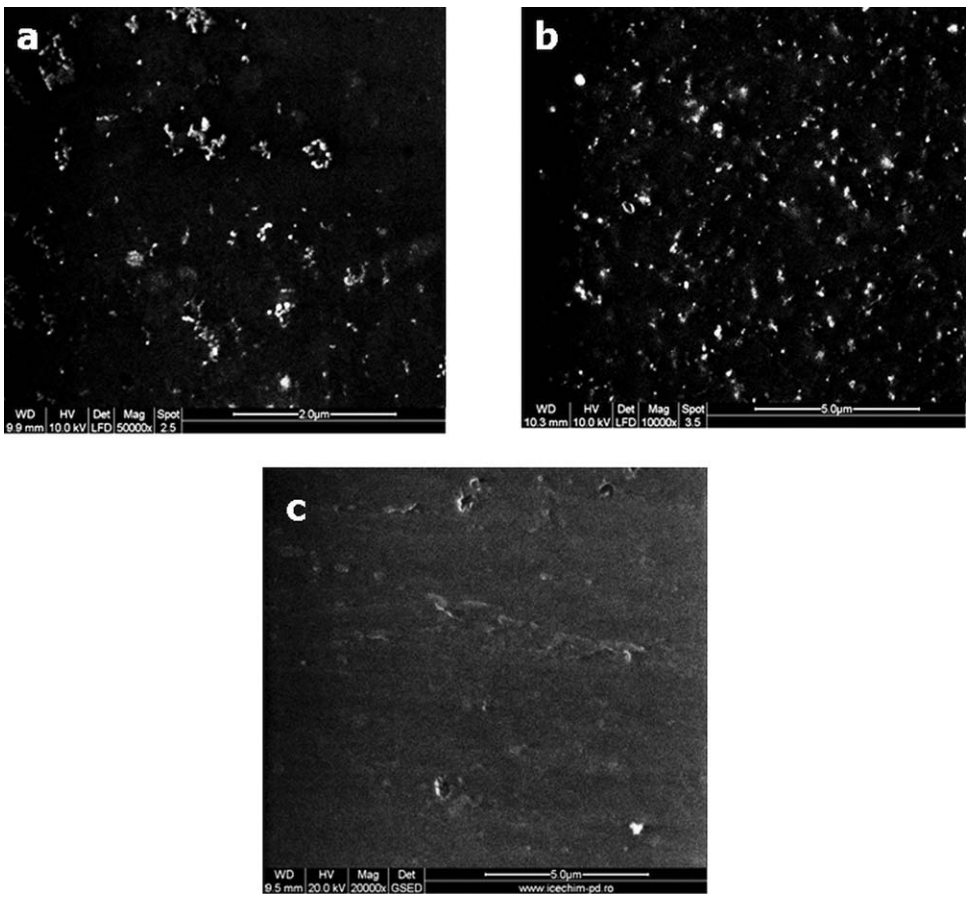

Figure 1 SEM images of samples: (a) PE/5% SiO_2 nanocomposite; (b) PE/5% Al_2O_3 nanocomposite; (c) neat PE.

MA-PE) [Fig. 2(b)] has a less-organized surface morphology.

AFM height images of silica and alumina nanocomposites are presented in Figure 2(c,d). Different morphologies can be seen in these images, including a fibrillar one for PE/SiO_2 nanocomposite and a granular structure in the case of nanoalumina composite. The fibrillar structure seems to be formed of grains, if a higher magnitude is considered [Fig. 2(e), detail]. The distribution of both nanofillers seems to be a nanolevel one. Nevertheless, it is difficult to analyze the dispersion of nanofillers in these images given the influence of the PE crystalline phase fine structure and surface irregularities. To overcome this difficulty, the already-pressed films of PE and nanocomposites were placed on Si wafers in the mold and maintained 5 min without pressure at 155–160°C, and then they were quickly quenched by immersion in cold water. This method have been already used by Tracz et al., who have obtained an attenuation of the crystalline phase in AFM imaging.[37] AFM 2D and 3D height images of quenched PE and PE nanocomposite samples are shown in Figures 3(a–d), 4(a–f), and 5(a–f). In these images, the brighter regions with respect to the surrounding area represent inorganic fillers and the more ordered material (crystalline structure) whereas the darker ones the less ordered, amorphous components.[35] Only neat PE [Fig. 3(a)] shows a lamellar structure, while all the other samples show less-ordered domains and a more or less deformed lamellar structure. It is to point out that the crystalline structure of the matrix (PE containing the compatibilizer) was not significantly modified by the incorporation of nanofillers in the case of quenched samples, individual grains of various sizes appearing in both Figures 3(b) and 4(a,d). Single oxide nanoparticles as well as agglomerates can be seen in both types of nanocomposites, but a better distribution seems to appear in the case of nanoalumina-containing composites as compared to nanosilica ones, after the comparison of a lot of samples. In the detailed image [Fig. 4(c)], the sequence of six nanosilica particles with a length of $\sim$ 600 nm, which form the agglomerate, is covered by a thin layer of less-organized polymer matrix, very close to the lamellar structured material. In Figure 4(f), the set of six nanoalumina particles that form the agglomerate with a length of $\sim$ 400 nm, are covered with polymer appearing as anchors on and between particles. Some tangential structures that anchors the nanofiller to the matrix are also seen in the case of silica nanoparticles and are attributed to

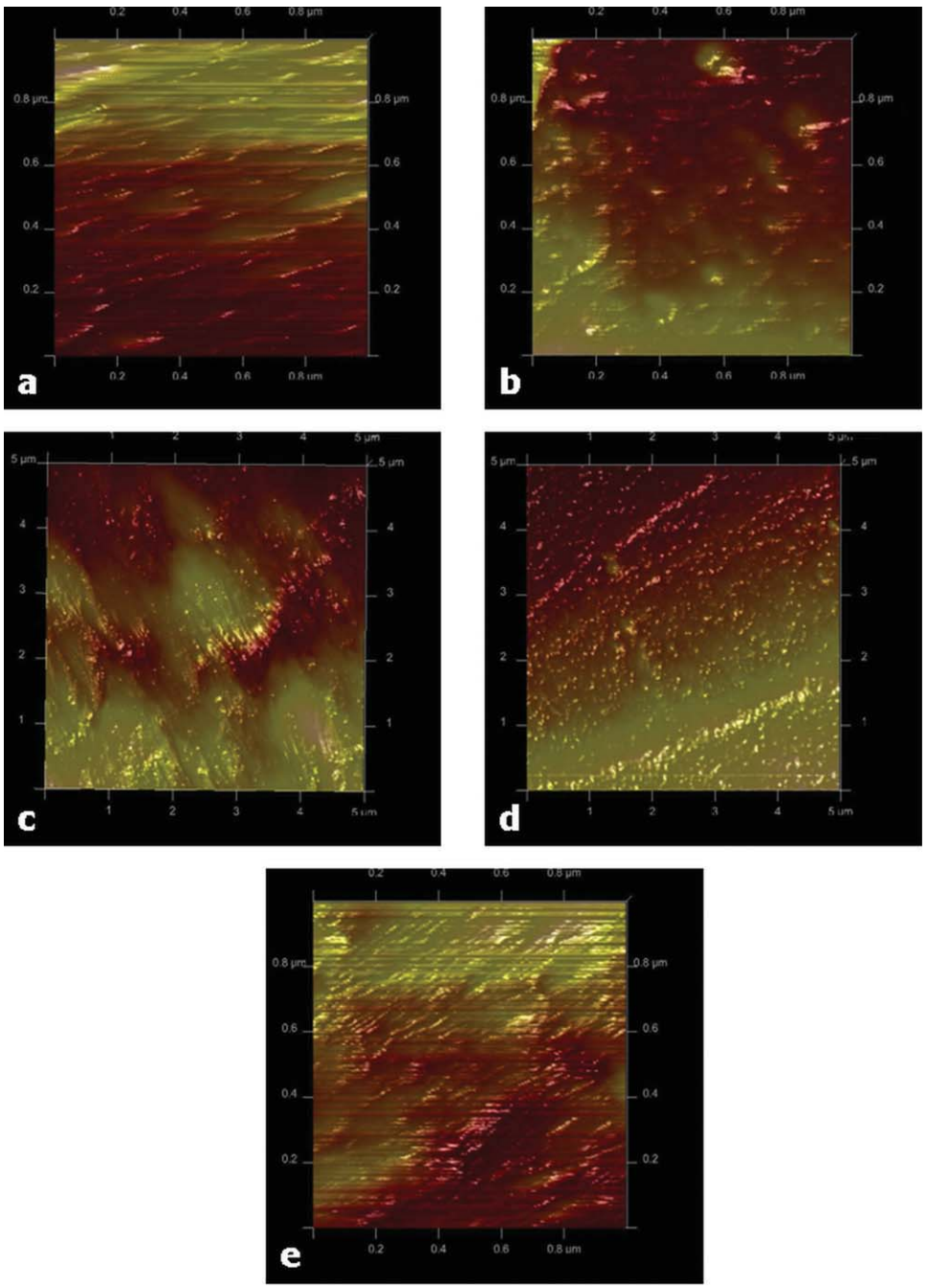

Figure 2 AFM height images of samples: (a) neat PE; scan size 1 μm × 1 μm; (b) the reference (PE + 5% MA-PE); scan size 1 μm × 1 μm; (c and e) PE/5% SiO_2 nanocomposite; scan size 5 μm × 5 μm and 1 μm × 1 μm for detail; (d) PE/5% Al_2O_3 nanocomposite; scan size 5 μm × 5 μm. [Color figure can be viewed in the online issue, which is available at wileyonlinelibrary.com]

compatibilizer chains.[35] The diameter of silica nanoparticles, determined based on AFM height images of PE/5% SiO_2 nanocomposite, was in a range from 10.7 to 79.3 nm with an average of 26.3 ± 7.6, and the diameter of alumina nanoparticles, in a range from 25.1 to 94.1 nm with an average of 45.8 ± 14.5 in the case of PE/5% Al_2O_3 nanocomposite, very close to the size of commercial alumina used in this study. A number of six different AFM height images were analyzed for each nanocomposite. The measurements were made using AFM software NanoScope version 1.20 in which the height of the nanoparticles or their agglomerates were determined. AFM particle analysis indicates a higher agglomeration grade of nanosilica particles in PE matrix.

WAXD analysis

X-ray diffraction analysis of filler nanopowders and thin film polymer samples was used to determine

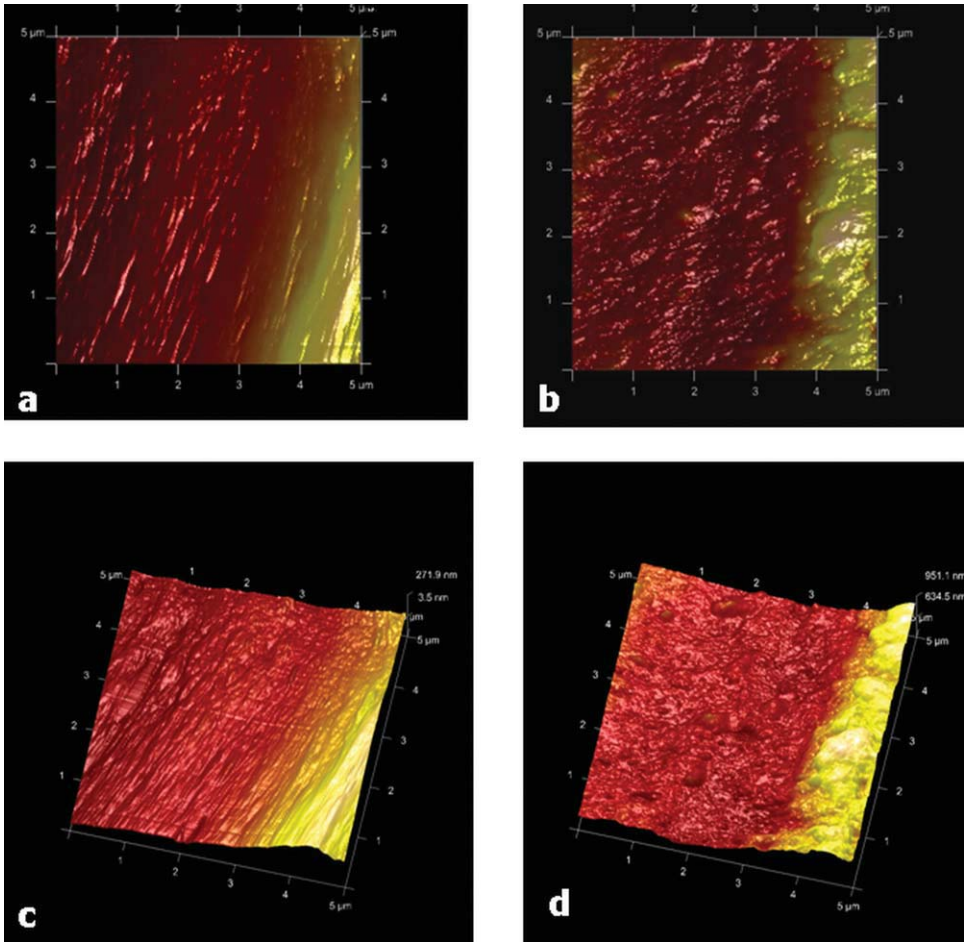

Figure 3 AFM height images of quenched samples (scan size 5 μm × 5 μm): (a) 2D image of neat PE; (b) 2D image of the reference (PE + 5% MA-PE); (c) 3D image of neat PE; (d) 3D image of the reference (PE + 5% MA-PE). [Color figure can be viewed in the online issue, which is available at wileyonlinelibrary.com]

the crystalline structure and the degree of crystallinity. Further results were obtained from the mediation of individual values obtained on four samples of the same material. The accuracy is ± 0.1% for interplanar distances, ± 1.5% for crystal dimension, and ± 2.0% for the index proportional to PE crystallinity (I_C). Crystals dimension of nanofillers was determined using the Scherrer Equation, which relates the peak breadth to the mean crystallite size.[38] The analysis of the WAXD diagrams of nano-oxides (not shown here) revealed that SiO_2 is entirely amorphous and Al_2O_3 is a mixture of γ and θ Al_2O_3. γ Al_2O_3 has a cubic structure with crystals dimension $\overline{D}_{100}$ = 117 Å, and θ Al_2O_3 a monoclinic structure with $\overline{D}_{111}$ = 120 Å. The average size of Al_2O_3 particles, given by the manufacturer (45 nm), is four times larger than the crystals, as resulted from WAXD analysis, which means that the crystals are sintered. The crystals dimensions of Al_2O_3 remain unchanged after their dispersion in melted polyethylene.

The WAXD diagrams of polyethylene filled with nano-SiO_2 (2 and 10 wt %) and nano-Al_2O_3 (same concentrations) are shown in Figure 6(a,b). Two main diffraction peaks appear in the polyethylene matrix at 2θ = 21.3° and 2θ = 23.7° corresponding respectively, to d_{110} and d_{200} in the orthorhombic system, as expected.[39] Polyethylene nanocomposites show the same peaks at the same 2θ as polyethylene indicating that the crystalline structure of the matrix remains unchanged upon blending with nano-SiO_2 or nano-Al_2O_3. The interplanar distances (d_{110} and d_{200}), integrated half width of the crystalline peaks (β_{110} and β_{200}), and the crystallite dimensions ($\overline{D}_{110}$ and $\overline{D}_{200}$) were calculated for all the samples and are presented in Table I. The interplanar distances (d_{110} and d_{200}) were calculated using the Bragg's relationship and the crystallite dimensions ($\overline{D}_{110}$ and $\overline{D}_{200}$) were calculated from the integrated half widths using the Scherrer Equation[40,41]:

$$\overline{D} = \frac{\lambda}{\beta_c \cos\theta} \tag{1}$$

where λ = 1.5406 Å, $\beta_c = \sqrt{\beta^2 - \beta_i^2}$ (β_i = instrumental half width), and θ is the diffraction angle (10.65°

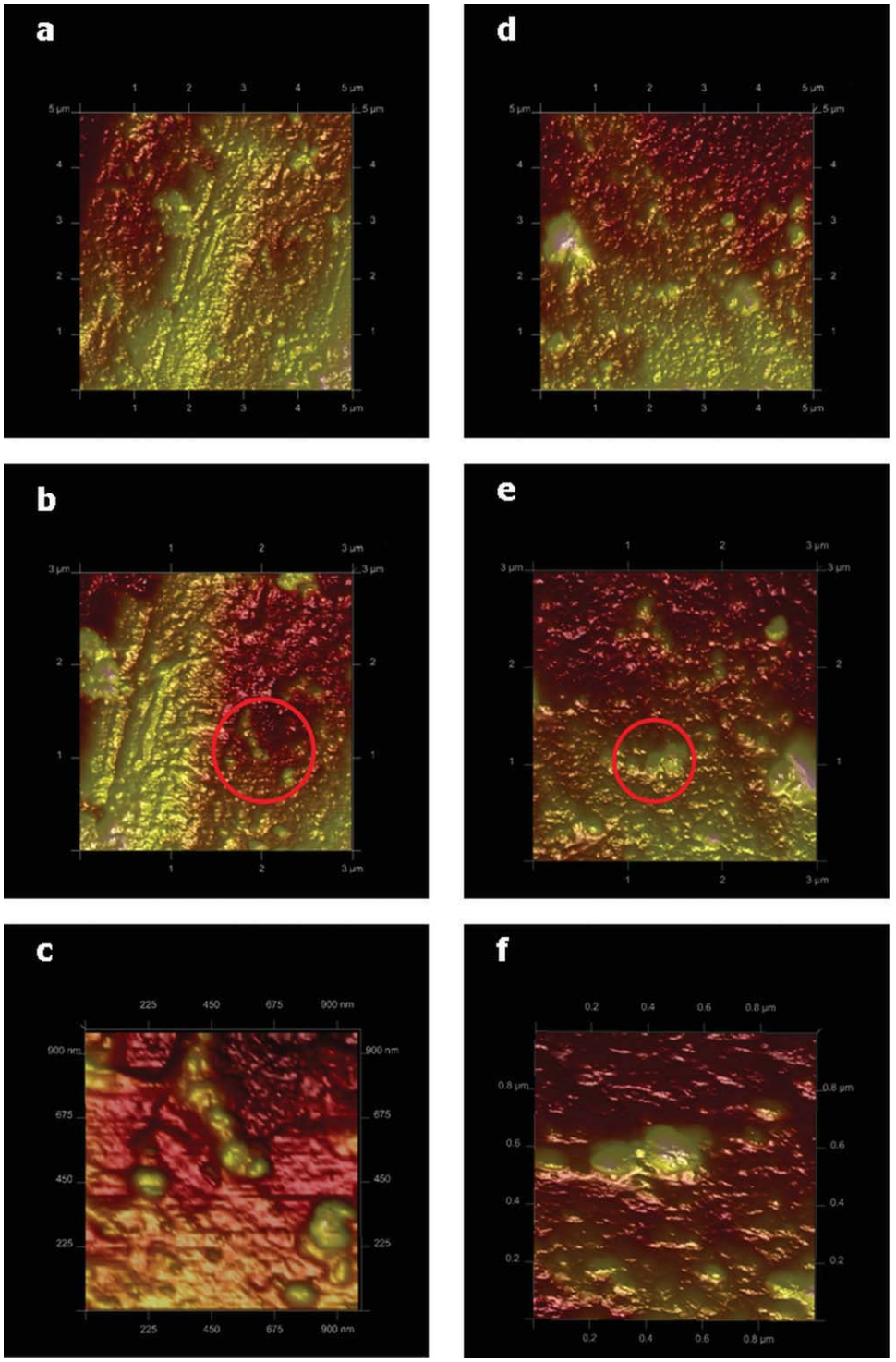

Figure 4 AFM 2D height images of quenched nanocomposite samples: (a–c) PE/5% SiO_2 scan size 5 μm × 5 μm, 3 μm × 3 μm, and 1 μm × 1 μm, respectively; (d–f) PE/5% Al_2O_3 scan size 5 μm × 5 μm, 3 μm × 3 μm, and 1 μm × 1 μm, respectively. [Color figure can be viewed in the online issue, which is available at wileyonlinelibrary.com]

and 11.85°, respectively). An increase of polyethylene crystallite mean dimensions, especially $\overline{D}_{110}$, is observed in both types of nanocomposites. This could be not only a result of the nucleating action of nanoparticles,[18] but also of the interactions between nano-oxides and amorphous polyethylene that hinders polymer crystallization (especially in the amorphous/crystalline space where small crystals are forming), resulting in less small crystals.

From Figure 6(a,b), a decrease of the intensity of PE crystalline peaks when adding nano-oxides (especially nano-SiO_2) can also be seen. The decrease

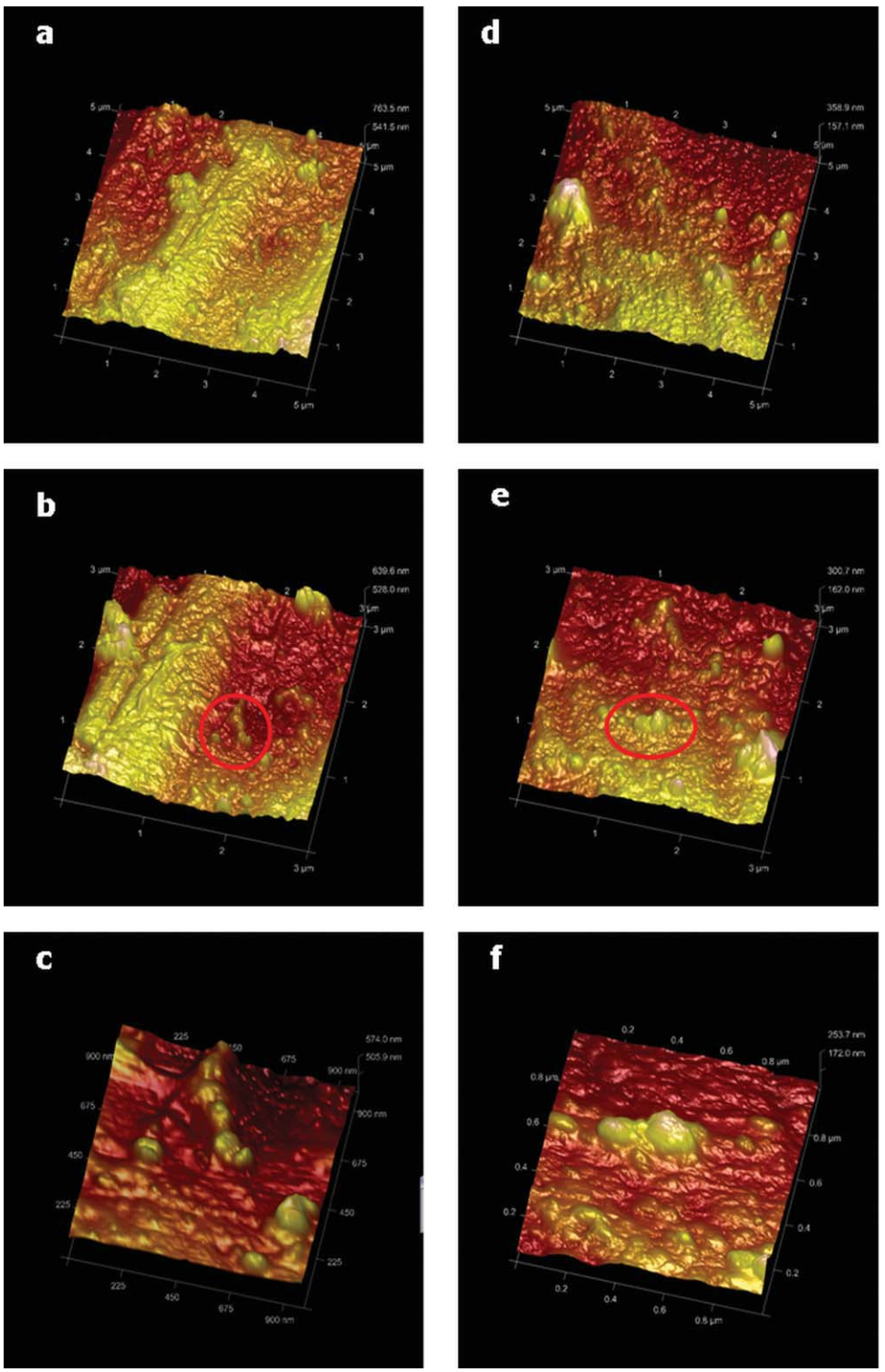

Figure 5 AFM 3D height images of quenched nanocomposite samples: (a–c) PE/5% SiO_2 scan size 5 μm × 5 μm, 3 μm × 3 μm, and 1 μm × 1 μm, respectively; (d–f) PE/5% Al_2O_3 scan size 5 μm × 5 μm, 3 μm × 3 μm, and 1 μm × 1 μm, respectively. [Color figure can be viewed in the online issue, which is available at wileyonlinelibrary.com]

in the peak intensity could be due to the higher absorption of nanoparticles that have higher density, and partially, to the decrease of crystallinity.[42] To verify this supposition, the WAXD crystallinity of polymer matrix, (I_C) was calculated as a ratio between the areas under the crystalline peaks and the total area (under the crystalline and amorphous peaks).[18,38] The amorphous peak of SiO_2 has been determined and taken out from the area of PE amorphous peak. I_C values, presented in Table I,

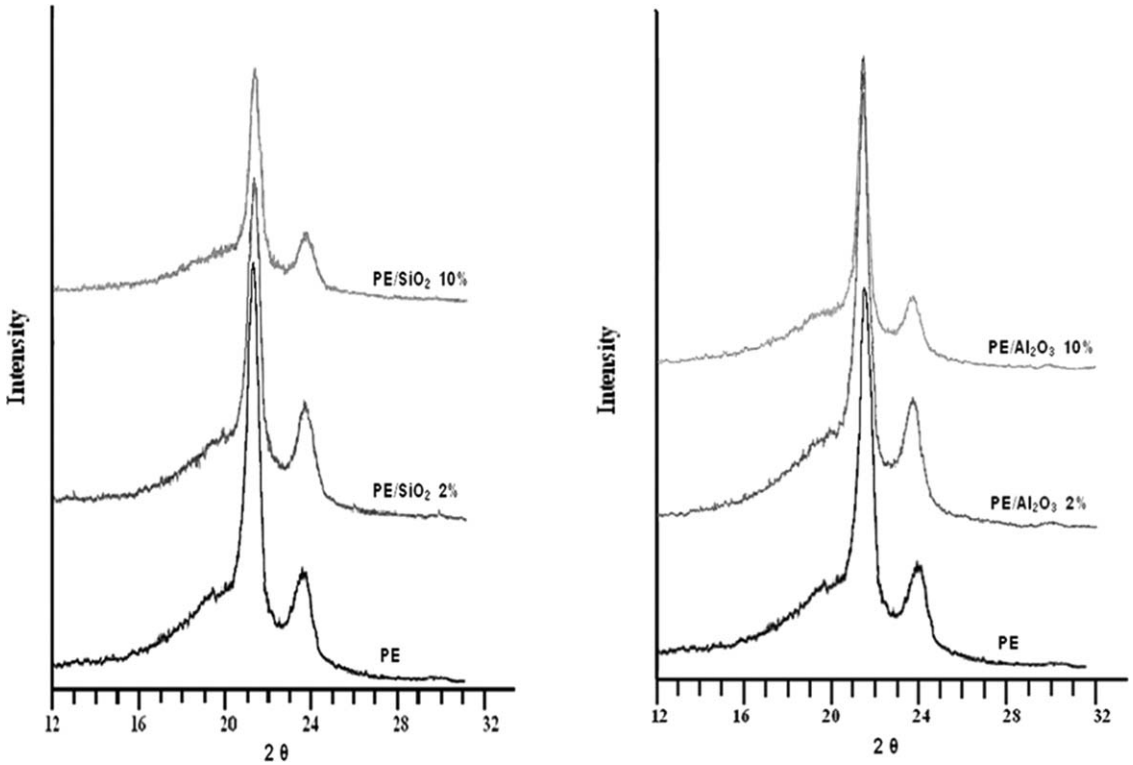

Figure 6 WAXD Diagrams of nanocomposites: left PE/SiO_2 with 0, 2, and 10% of nanosilica; right PE/Al_2O_3 with 0, 2, and 10% of nanoalumina.

highlight a decrease of PE crystallinity with the increasing amount of nanosilica, but no important change of PE crystallinity for nano-Al_2O_3 composites. Some early studies have evidenced a similar behavior, that is, a decrease of the crystallinity of LDPE and other polyolefins when 2, 4, and 8 vol % nanosilica of 7-nm diameter was added.[43] A different behavior was signaled in the case of linear LDPE containing low concentration (under 4 wt %) of 16-nm silica nanoparticles, treated with dimethyldichlorosilane, materialized in an increase of polyethylene crystallinity.[44] No influence of nano-Al_2O_3 particles (47 nm) on PP crystallinity was noted by Zhao and Li.[45] These data reveal a different behavior of nano-oxides depending on the polymer and treatment. Therefore, the nature and the intensity of the interactions occurring at the nanoparticle–polyethylene interface are different for the two nanofillers. The decrease of PE crystallinity in our composites could be explained by the effect of 15-nm silica nanoparticles in hindering the motion of the polymer chain segments and crystallization process as well. At the same percentage of filling, the effect of nano-Al_2O_3 (45 nm) will be less important, due to the difference in density compared to nano-SiO_2 (3.5 up against 2.2) and to the difference of specific surface area (40 up against 180). DSC measurements are necessary to prove this reasoning.

Another observation must be noted: although the crystallinity of the matrix decreases when nano-SiO_2 is added, the crystal dimension increases. A similar result was obtained by Hui et al.[18] in the case of a LDPE /ethylene vinyl acetate copolymer filled with 15-nm SiO_2. This behavior was explained as a

TABLE I
WAXD Results for PE/Nano-Oxides Composites

Samples	$d_{110} \pm 0.1\%$ (Å)	$\overline{D}_{110} \pm 1\%$ (Å)	$d_{200} \pm 0.1\%$ (Å)	$\overline{D}_{200} \pm 1\%$ (Å)	$I_C \pm 1\%$ (%)
PE	4.171	125	3.759	100	43.6
PE/SiO_2 2 wt %	4.152	127	3.745	98	42.3
PE/SiO_2 5 wt %	4.147	147	3.747	101	40.8
PE/SiO_2 10 wt %	4.156	140	3.748	106	38.9
PE/Al_2O_3 2 wt %	4.173	140	3.760	100	43.0
PE/Al_2O_3 5 wt %	4.169	135	3.749	99	43.3
PE/Al_2O_3 10 wt %	4.167	143	3.751	110	43.0

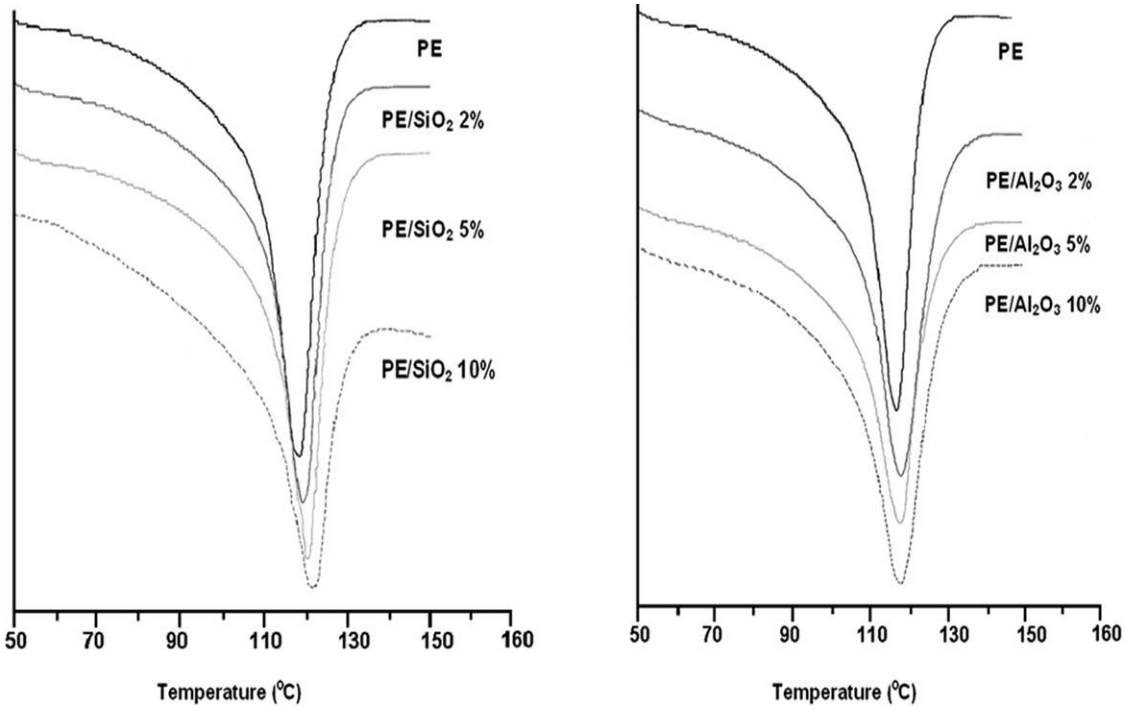

Figure 7 DSC diagrams of PE and PE nanocomposites (left with nano-SiO_2, right with nano-Al_2O_3).

consequence of the small dimension of SiO_2 nanoparticles that may locate in the interlamellar spaces in the polymer matrix inhibiting the crystallization but, because of their nucleating action, they may contribute to the increase of crystal dimension.

DSC analysis

DSC was carried out on the same polyethylene samples to estimate the effect of nanosilica and nanoalumina on PE crystallinity (Fig. 7). Thermal properties—melting point (T_m) and heat of fusion (ΔH)—were also determined. The degree of crystallinity X_C was calculated from DSC curves as follows:

$$X_C = \frac{\Delta H}{\Delta H_0 w_{\mathrm{PE}}} \cdot 100 \qquad (2)$$

where ΔH is the heat of fusion for the composite, ΔH^0 is the heat of fusion for completely crystallized PE (289.9 J/g[46]), and w is the weight fraction of polymer matrix.

DSC results are given in Table II. A crystal melting peak (T_m) at 117.0°C associated with crystalline PE appears in the case of the matrix. MA-PE is almost entirely amorphous. In the presence of nanosilica, a slight increase of T_m is observed. A high nano-SiO_2 content (10%) induces an increase with 5° of T_m, from 117.0°C for the matrix to 122.2°C for the composite. Nanoalumina composites exhibit slightly higher temperatures compared with the matrix, an influence of nanoalumina loading being not visible. The slight increase in T_m could indicate an improvement of polymer/filler interface properties and is correlated with the increased size of crystals.

TABLE II
DSC Results for PE/Nano-Oxides Composites

Samples	Melting peak temperature $T_m \pm 0.5$ (°C)	Heat of fusion $\Delta H \pm 1\%$ (J/g)	Degree of crystallinity $X_C \pm 1.5\%$ (%)
PE	117.0	98.0	35.6
MA-PE	105.2	2.4	0.9
PE/SiO_2 2 wt %	117.1	91.1	33.8
PE/SiO_2 5 wt %	118.8	86.8	33.3
PE/SiO_2 10 wt %	122.2	80.3	32.6
PE/Al_2O_3 2 wt %	118.6	92.1	34.2
PE/Al_2O_3 5 wt %	118.1	89.5	34.3
PE/Al_2O_3 10 wt %	118.3	83.8	34.0

PE crystallinity slightly decrease in the case of nanocomposites as compared to neat PE (Table II), but the difference regarding the influence of silica and alumina nanoparticles on polyethylene crystallinity is less important as in the case of WAXD analysis. However, polyethylene crystallinity depend on the processing conditions, especially hot pressing parameters, knowing that the balance between amorphous and crystalline fractions can be adjusted by thermal methods.

The possible changes in polymer morphology due to the presence of the nanofillers could also be explained by considering a multicore model for the nanoparticle–polymer interface, proposed by Tanaka et al.[47] According to this model, the nanofiller–polymer interface may consist of three layers called bonded layer, bound layer, and loose layer, as well as an electric double layer that overlaps the above three layers. The first layer is a transition region that tightly bonds the inorganic nanoparticle to the outer polymer matrix, usually by compatibilizing agents. The second and the third layer are attributed to different chain conformation, chain mobility, free volume, and crystallinity of the polymer matrix, the second layer being an intermediate layer with a rather ordered structure whereas the third layer showing a rather amorphous morphology. This nanostructure model is very close to the architecture observed in AFM images. Accordingly, discussing our results on material morphology by taking into account the above described multicore model of Tanaka, the decrease of the crystallinity with the nanofiller content could be the result of the increase of the volume occupied by the third layer of the polymer–filler interface, while the increase of the crystal dimension appears to be in agreement with the increase of the region corresponding to the second layer of the interface.

Mechanical characterization

The relative tensile modulus E/E_0 (E—tensile modulus of elasticity of the composite and E_0—the value for PE matrix) as a function of nanofiller content is shown in Figure 8. An increase of tensile modulus with nano-oxides content is observed, resulting in a net rise of about 2.5 times for 2 wt % nano-oxides and of 2.8 times for 10 wt % SiO_2 or Al_2O_3, over unfilled PE. Therefore, both types of nano-oxides are able to stiffen the polymer matrix. These results indicate a reinforcing effect of the nanoparticles on the polymeric matrix and, therefore, an appropriate level of interfacial bonding between SiO_2 or Al_2O_3 nanoparticles and polyethylene, effect favored by MA-PE used as compatibilizing agent. The largest increase can be observed at low content of nano-oxides, up to 2%. This can be explained by a better dispersion of

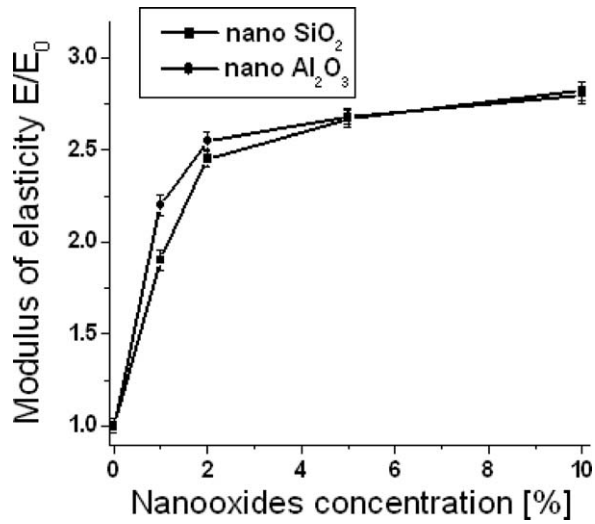

Figure 8 Relative tensile modulus of PE/nano-oxides composites.

low nano-oxides concentrations in polyethylene by maleic anhydride graft polyethylene. The effect of the compatibilizing agent (same concentration in all samples) in improving mechanical properties of nanocomposites is more evident at low nano-oxides content, because it seems the amount of MA-PE is properly distributed at polyethylene/nano-oxide interface in this case, providing a better dispersion of the filler and a stronger interface. The higher number of Si—C—O bonds produced through dehydration of hydroxyl groups in MA-PE with residual silanol groups in the silica network contributes to a stronger interface in this case. To verify this supposition, a complementary sample containing the same additives, in the same concentration as PE/5% SiO_2 but with a double concentration of MA-PE was prepared in the same conditions. A higher relative modulus was obtained in this case (2.97 MPa for 10% MA-PE instead of 2.67 MPa for 5% MA-PE), indicating the increasing influence of compatibilizing agent content on interface properties.

Tensile strength and elongation at break of PE/SiO_2 and PE/Al_2O_3 nanocomposites versus nanofiller concentration are presented in Figures 9 and 10. A slight increase (up to 15%) of both tensile strength and elongation at break can be observed for a small content of nano-oxides in PE, up to 2 wt %. A similar behavior was signaled for treated silica nanoparticles in PP.[19,48] Simultaneous rises in modulus, tensile strength, elongation at break, and impact strength were observed in the case of PP composites containing polybutyl acrylate grafted silica nanoparticles in small concentration, up to 3 wt %.[19] This behavior may be explained by a stronger filler/matrix adhesion in the case of a suitable treatment for silica nanoparticles. The higher elongation values of these composites are the result of the plastic

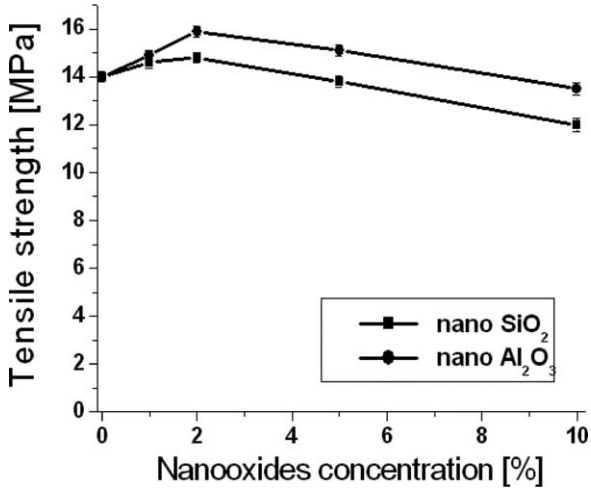

Figure 9 Tensile strength of PE/nano-oxides composites.

deformation of a large amount of PP matrix beside the grafted nanoparticles induced under the applied force.[19] In the case of polyethylene nanocomposites, it seems a similar behavior has not yet been signaled.

A clear decrease of the tensile strength and, especially, of the elongation at break, is noticed at more than 5 wt % nano-SiO_2 in polyethylene. In the same range of concentrations (5–10%), only a slow decrease of these tensile characteristics can be remarked for PE/Al_2O_3 nanocomposites. For both types of composites, a maximum peak of the tensile strength and elongation is observed at a nano-oxide content of $\sim$ 2 wt % (Figs. 9 and 10). A similar behavior was observed in the case of PP/nanosilica composites.[48] Typical tensile stress–strain curves of neat PP and PP filled with SiO_2-g-PS nanoparticles show a simultaneous increase in stiffness and ductility.[48] This behavior was explained by the uniform dispersion and distribution of the filler in the matrix as well as by a better interfacial adhesion. In the case of considered composites, low filler content seems to be beneficial both from the stand point of the dispersion of nano-oxides in PE and the efficiency of the compatibilizing agent, as above specified for modulus. With increasing filler content, in the case of a good dispersion, the interfacial area should increase, especially in PE/SiO_2 nanocomposites because of the smaller size of nanosilica as compared with nanoalumina. When nanoparticle agglomerates appear, as for PE/5% SiO_2 in SEM and AFM images, beneficial effect of smaller sizes of nanoparticles will be offset by nanoparticles agglomeration so that the interfacial area will be lower, affecting mechanical properties. The results of mechanical tests show that the nanofiller dispersion and the adhesion at interface are the best at 2 wt % nano-oxides in polyethylene.

The significant decrease of the elongation at break, as observed for PE/10% SiO_2 nanocomposite, could suggest the occurrence of a transition in the deformation mode. Bazhenov et al. has signaled a ductile-to-quasi-brittle transition for calcium carbonate filled amorphous copolyester, which arises at about 14 vol % of micron size filler,[49] much higher than the concentration range considered in our experiments. Our tensile stress–strain curves of nanosilica-filled polyethylene composites are shown in Figure 11. After reaching the yield point, the stress remained almost constant while the neck is propagating through the entire gauge length of the specimen and then increases till the breaking. This behavior is similar to PE sample, as well as PE with 1, 2, and 5% nanosilica. Accordingly, in case of 10% of filler, the fracture occurred in the final stage of neck propagation or at the beginning of strain hardening. This can indicate

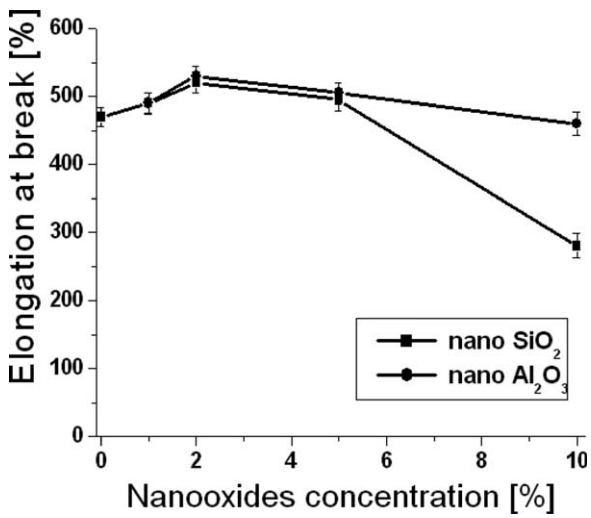

Figure 10 Elongation at break of PE/nano-oxides composites.

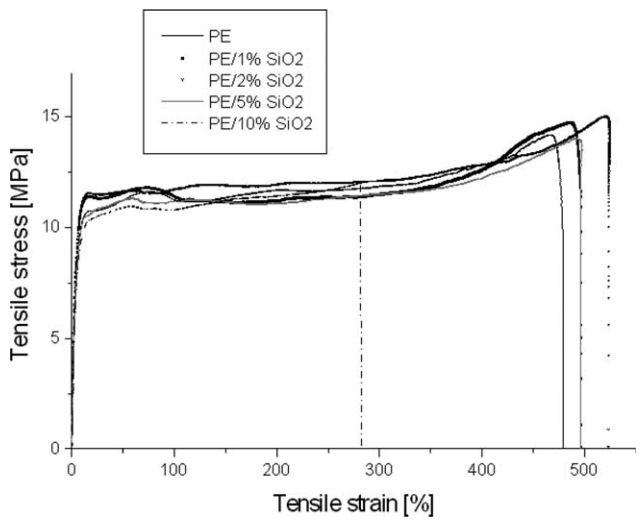

Figure 11 Typical tensile stress–strain curves of neat PE and PE filled with nano-SiO_2.

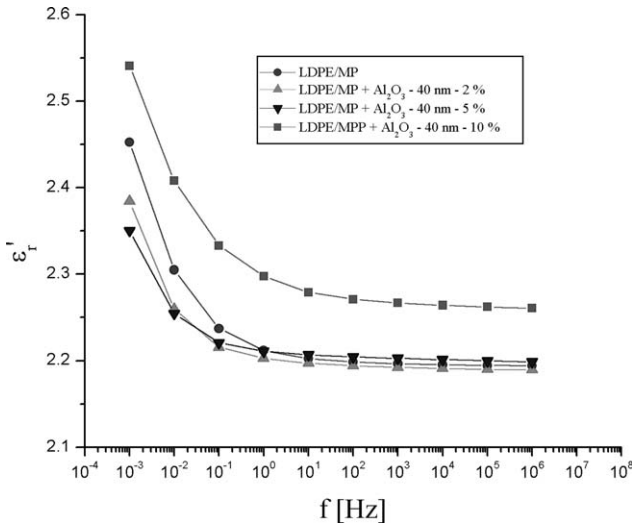

Figure 12 ε_r' versus frequency for PE/Al_2O_3 nanocomposites at different filler concentrations.

a certain influence of the amount of nano-like particles or an inherent decrease of interfacial adhesion given the lower ratio of the compatibilizing agent to the nanofiller amount as discussed above.

Characterization by dielectric spectroscopy

Dielectric spectroscopy was conducted for the base polymer and polyethylene nanocomposites with SiO_2 and Al_2O_3 nanoparticles. The dielectric spectroscopy results revealed, on the one hand, the influence of the filler content and, on the other hand, the effect of the filler type on the change in permittivity as a function of frequency at 25°C. The influence of nanoalumina content on the dielectric behavior can be seen in Figure 12, which shows the change in ε_r' (the real part of the complex relative permittivity) with the nano-Al_2O_3 concentration in the frequency range f: 10^{-3} to 10^6 Hz. The sharp decrease of ε_r' with the frequency at low values of f and slight decrease at $f > 1$ Hz was also observed in other studies.[50–52] This behavior was called anomalous low frequency dispersion by Jonscher[53] and quasi-dc behavior (QDC) by Dissado and Hill.[54] For very low frequencies (10^{-3} to 10^{-1} Hz), ε_r' values for the polyethylene nanocomposites with 2 and 5 wt % filler content are smaller than for the unfilled polyethylene. This could arise from a reduced chain movement inside the second layer of the nanofiller–polymer interface and to the reduction of the free volume in the third layer of the interface of the polymer in the nanocomposite with respect to the unfilled polyethylene. The ε_r' values for 10 wt % nano-Al_2O_3 in polyethylene are higher than both unfilled polymer and filled with 2 and 5 wt % nanofiller, probably due to a major contribution of the interfacial polarization, determined by the increased number of charges (impurities and small ions) introduced in the polymer with the nanoparticles. This behavior could also be explained by a good dispersion of small concentration of nanofiller and by the presence of small agglomerations at high nano-Al_2O_3 concentration in polyethylene.

In the case of PE/SiO_2 nanocomposites (Fig. 13), the presence of the nanoparticles leads to an increase of the permittivity values with respect to the unfilled polyethylene for a broad range of frequencies (10^{-3} to 10^3 Hz). This increase becomes more important with the increase of SiO_2 nanoparticles concentration, which determines an increase of the number of dipoles and an intensification of the interfacial polarization. Once again, the ε_r' values for 10 wt % nano-SiO_2 in polyethylene are higher than both unfilled polymer and filled with 2 and 5 wt % nanofiller, same as in the case of 10% nanoalumina composites. Another remark at these nanocomposites is the occurrence of a perturbation in the frequency variation of ε_r' at about 10^3 Hz, showing a dielectric relaxation due to presence of the nanoparticles (Fig. 13).

Although a clear relation between the crystallinity degree and dielectric properties could not be done, the decrease of PE crystallinity with the increase of nanosilica concentration coincides with the increase of the PE/silica nanocomposites permittivity in function of nanosilica content for a given frequency. This suggests an increase of the volume of the third layer of the polymer–nanofiller interface and consequently of the contribution of this layer to the material polarization with the nanofiller content. Thus, the volume occupied by this loose layer becomes larger with the increase of the nanofiller content, leading to an increase of the number of impurities, ions, dipolar species, molecule fragments, which determines an

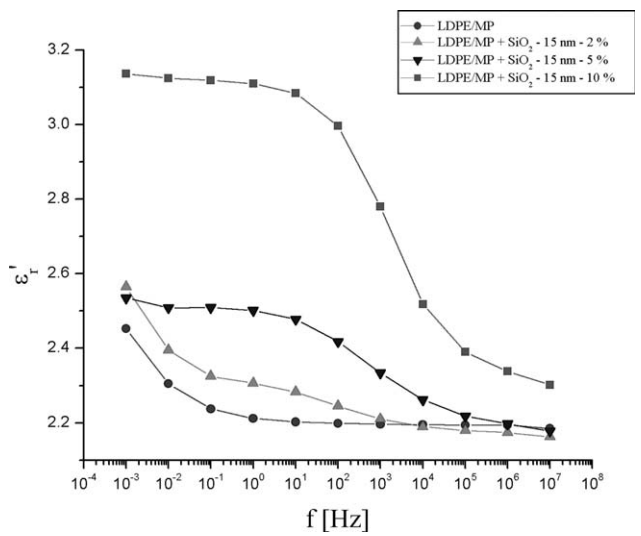

Figure 13 ε_r' versus frequency for PE/SiO_2 nanocomposites at different filler concentrations.

TABLE III
Filler Characteristics in PE/Nano-Oxides Composites

Nanocomposite type	Mass fraction (wt %)	Volume fraction (% v/v)	Average interparticle distance[a] (nm)	Total interface area[a] (km^2/m^3)
PE/SiO_2	2	0.85	44.99	3.40
	5	2.17	29.79	8.68
	10	4.46	21.29	17.84
PE/Al_2O_3	2	0.54	167.01	0.72
	5	1.37	115.23	1.83
	10	2.85	87.15	3.79

[a] Calculated according to Ref. 47.

increase of the ionic, orientation, and interfacial polarizations.

Regarding the effect of the filler type on the permittivity, one can remark different behaviors especially for low nanofiller content. Thus, in the case of polyethylene nanocomposites with 2 or 5 wt % Al_2O_3, the values of the permittivity are smaller than for the unfilled polymer, whereas in the case of nanocomposites with 2 or 5 wt % SiO_2, the values of the permittivity are higher than for the unfilled polymer up to $f = 5$ kHz. Another difference is the relaxation observed for the nanocomposites with SiO_2 fillers, which is not detected in the case of Al_2O_3 nanofillers. A possible explanation for this different behavior could be the larger average interparticle distance and the smaller filler volume fraction when using Al_2O_3 than in the case of SiO_2 filler (Table III), which could determine that a possible relaxation for the nanocomposites with Al_2O_3 nanofiller be undetectable for the concentrations used in our experiments. The average interparticle distance (D) was calculated according to Ref. 47 by using the following relations:

$$D = \left\langle \left\{ \frac{\pi}{6} \left(\frac{\rho_n}{\rho_m} \right) \frac{100}{\text{wt\%}} \left[1 - \frac{\text{wt\%}}{100} \left(1 - \frac{\rho_m}{\rho_n} \right) \right] \right\}^{\frac{1}{3}} - 1 \right\rangle d \tag{3}$$

$$S = 6V_f/d \tag{4}$$

where d, V_f, and S are a particle diameter, a filler volume fraction, and the total interface area per unit volume, respectively, and ρ_n and ρ_m are the density of nanofiller and polymer matrix, respectively.

From the Figures 12 and 13 it can be seen that for the same nanofiller mass fraction at a particular frequency, ε_r' values for PE/nanosilica composites are higher than the values obtained for PE/nanoalumina composites, even if the permittivity of silica (≈ 4) is smaller than the permittivity of alumina (≈ 10). This behavior emphasizes the important role of the nanofiller–polymer matrix interface. Thus, the effect of the polarization in the interface area (larger in the case of silica filler than in the case of alumina filler (Table III)) is more important than the effect of the polarization inside nanoparticles.

CONCLUSIONS

Morphological, mechanical, and electrical characteristics of polyethylene nanocomposites with nano-SiO_2 and nano-Al_2O_3 were studied to gain some insight into the way in which these composites may behave as a preliminary step to nanodielectrics design.

Both types of considered nano-oxides induce changes in the morphology, mechanical, and electrical characteristics of polyethylene. The changes in the polyethylene morphology induced by nano-oxides and revealed by WAXD analysis, consist in a small decrease of PE crystallinity in the case of nanosilica-containing composites, and in an increase of polyethylene crystallite mean dimensions for both types of nanofillers. A dispersion at nanolevel of both SiO_2 and Al_2O_3 nanoparticles in polyethylene is revealed by SEM, with a better dispersion for nano-Al_2O_3.

The structural organization in polyethylene nanocomposites and the dispersion of the nano-oxides in the matrix, visualized by AFM revealed a lamellar ordered structure in neat polyethylene and a less organized structure and a top layer of an amorphous phase in the case of polyethylene containing the compatibilizer. Different fibrillar and granular morphologies were observed in the AFM images of nanosilica- and nanoalumina-containing composites, in the quenched samples the crystalline structure of the matrix (PE containing the compatibilizer) was not significantly modified by the incorporation of nanofillers. Moreover, the AFM particle analysis indicates a higher degree of agglomeration of nanosilica particles, similar to SEM observations.

A reinforcing effect of both types of nano-oxides in polyethylene was observed from the important

increase of the tensile modulus, especially for low nano-oxides concentration (2 wt %), where an increase of both tensile strength and elongation at break was noticed. The best mechanical properties at low filler content were explained by a more favorable dispersion of nanofiller as well as an increased adhesion at the interface.

The results of dielectric characterization emphasize different dielectric behaviors of the nanocomposites, depending on the frequency and on the nanofiller concentration and type. Smaller permittivity values than those of the base polymer were observed for PE nanocomposites with a low content of Al_2O_3 (2 wt %) at very low frequencies. Besides dielectric features, the improvement of the mechanical properties is also important, because an insulating material might be subjected to complex loading including vibration, abrasion, and high shear stress. PE/2% nano Al_2O_3 composite shows improved mechanical and dielectric properties over pure polyethylene and is very interesting for applications in the electrical power industry. Several nanocomposites prepared and characterized in this study display balanced mechanical–dielectric properties, indicating potential application in the electrical insulation industry for AC and DC high, medium, or low voltage.

This work was performed in the frame of CEEX-PoNaDIP-234/2006.

References

1. Shelley, J. S.; Mather, P. T.; DeVries, K. L. Polymer 2001, 42, 5849.
2. Jordan, J.; Jacob, K. I.; Tannenbaum, R.; Sharaf, M. A.; Jasiuk, I. Mater Sci Eng A 2005, 393, 1.
3. Nair, S. V.; Goettler, L. A.; Lysek, B. A. Polym Eng Sci 2002, 42, 1872.
4. Ash, B. J.; Roger, D. F.; Wiegand, C. J.; Schadler, L. S.; Siegel, R. W.; Benicewicz, B. C.; Apple, T. Polym Compos 2002, 23, 1014.
5. Siengchin, S.; Karger-Kocsis, J.; Thomann, R. J Appl Polym Sci 2007, 105, 2963.
6. Osman, M. A.; Atallah, A. Macromol Rapid Commun 2004, 25, 1540.
7. Reynaud, E.; Jouen, T.; Gauthier, C.; Vigier, G.; Varlet, J. Polymer 2001, 42, 8759.
8. Stoeffler, K.; Lafleur, P. G.; Denault, J. Polym Eng Sci 2008, 48, 2459.
9. Lee, Y. H.; Wang, K. H.; Park, C. B.; Sain, M. J Appl Polym Sci 2007, 103, 2129.
10. Arunvisut, S.; Phummanee, S.; Somwangthanaroj, A. J Appl Polym Sci 2007 106, 2210.
11. Passaglia, E.; Bertoldo, M.; Coiai, S.; Augier, S.; Savi, S.; Ciardelli, F. Polym Adv Technol 2008, 19, 560.
12. Qian, Z.; Zhou, H.; Xu, X.; Ding, Y.; Zhang, S.; Yang, M. Polym Compos 2009, 30, 1234.
13. Sharma, S. K.; Nema, A. K.; Nayak, S. K. J Appl Polym Sci 2010, 115, 3463.
14. Chrissafis, K.; Paraskevopoulos, K. M.; Tsiaoussis, I.; Bikiaris, D. J Appl Polym Sci 2009, 114, 1606.
15. Nagy, J. B.; US Patent 7,223,811, 2007.
16. Ren, X.; Wang, X. Q.; Sui, G.; Zhong, W. H.; Fuqua, M. A.; Ulven, C. A. J Appl Polym Sci 2008, 107, 2837.
17. Rong, M. Z.; Zhang, M. Q.; Pan, S. L.; Lehmann, B.; Friedrich, K. Polym Int 2003, 53, 176.
18. Hui, S.; Chaki, T. K.; Chattopadhyay, S. J Appl Polym Sci 2008, 110, 825.
19. Wu, C. L.; Zhang, M. Q.; Rong, M. Z.; Friedrich, K. Compos Sci Technol 2005, 65, 635.
20. Zhang, M. Q.; Rong, M. Z.; Zhang, H. B.; Friedrich, K. Polym Eng Sci 2003, 43, 490.
21. Wang, W.-Y.; Zeng, X.-F.; Wang, G.-Q.; Chen, J.-F. J Appl Polym Sci 1932, 2007, 106.
22. Parsonage, E.; US Patent 7,591,831, 2009.
23. Eteläaho, P.; Nevalainen, K.; Suihkonen, R.; Vuorinen, J.; Järvela, P. J Appl Polym Sci 2009, 114, 978.
24. Lewis, T. J. IEEE Trans Diel Electr Insul 1994, 1, 812.
25. Nelson, J. K.; Fothergill, J. C. Nanotechnology 2004, 15, 586.
26. Ma, D.; Siegel, R. W.; Hong, J.-I.; Schadler, L. S.; Martensson, E.; Önneby, C. J Mater Res 2003, 19, 857.
27. Nelson, J. K.; Breakdown Strength of Solids, In: Engineering Dielectrics, Vol. 2A, Bartnikas, R.; Eichhorn, R.M. editors, ASTM Publication Philadelphia, PA 1993.
28. Lewis, T. J. IEEE Trans Diel Electr Insul 2004, 11, 739.
29. Jianwen, X.; Wong, C. P. Compos Part A Appl Sci Manuf 2007, 38, 13.
30. Chen, G.; Tanaka, Y.; Takada, T.; Zhong, L. IEEE Trans Diel Electr Insul 2004, 11, 113.
31. Nakayama, N.; Hayashi, T. J Appl Polym Sci 2007, 105, 3662.
32. Roy, M.; Nelson, J. K.; Schadler, L. S.; Zou, C.; Fothergill, J. C. Annual Report—Conference on Electrical Insulation and Dielectric Phenomena, CEIDP '05 2005, IEEE Publication Department, Piscataway, NJ, 183.
33. Nelson, J. K.; US Patent 7,579,397, 2009.
34. Tjong, S. C.; Liang, G. D.; Bao, S. P. J Appl Polym Sci 2006, 102, 1436.
35. Magonov, S. N. In Encyclopedia of Analytical Chemistry; Meyers, R. A., Ed.; Wiley: Chichester, 2000, p 7432.
36. Ma, D.; Akpalu, Y. A.; Li, Y.; Siegel, R. W.; Schadler, L. S. J Polym Sci B Polym Phys 2005, 43, 488.
37. Tracz, A.; Jeszka, J. K.; Kucinska, I.; Chapel, J.-P.; Boiteux, G.; Kryszewski, M. J Appl Polym Sci 2002, 86, 1329.
38. Yeh, S. W.; Wu, T. L.; Wei, K. H.; Sun, Y. S.; Liang, K. S. J Polym Sci B Polym Phys 2005, 43, 1220.
39. Yoo, S.; Lee, J.; Holloman, C.; Pascall, M. A. J Appl Polym Sci 2009, 112, 107.
40. Liu, L.-Z.; Hsiao, B. S.; Ran, S.; Fu, B. X.; Toki, S.; Zuo, F.; Tsou, A. H.; Chu, B. Polymer 2006, 47, 2884.
41. Yang, D. C.; Thomas, E. L. J Mater Sci 2098, 1984, 19.
42. Huang, J.-W.; Wen, Y.-L.; Kang, C.-C.; Tseng, W.-J.; Yeh, M.-Y. Polym Eng Sci 2008, 48, 1268.
43. Kalfus, J.; Jancar, J.; Kucera, J. Polym Eng Sci 2008, 48, 889.
44. Kontou, E.; Niaounakis, M. Polymer 2006, 47, 1267.
45. Zhao, H.; Li, R. K. Y.; Proceedings of the 11th International Conference on Fracture, Italy 2005, 74.
46. Xia, X.; Xie, C.; Cai, S. Thermochim Acta 2005, 427, 129.
47. Tanaka, T.; Kozako, M.; Fuse, N.; Ohki, Y. IEEE Trans Diel Electr Insul 2005, 12, 669.
48. Zhang, M. Q.; Rong, M. Z. Chinese J Polym Sci 2003, 21, 587.
49. Bazhenov, S.; Li, J. X.; Hiltner, A.; Baer, E. J Appl Polym Sci 1994, 52, 243.
50. Roy, M.; Nelson, J. K.; Reed, C. W.; MacCrone, R. K.; Keefe, R. J.; Zenger, W.; Schadler, L. S. IEEE Trans Diel Electr Insul 2005, 12, 629.
51. Singha, S.; Thomas, M. J. IEEE Trans Diel Electr Insul 2008, 15, 2.
52. Maity, P.; Poovamma, P. K.; Basu, S.; Parameswaran, V.; Gopta N. IEEE Trans Diel Electr Insul 2009, 16, 1481.
53. Jonscher, A. K. Dielectric Relaxation in Solids; Chelsea Dielectric Press, London, 1983.
54. Dissado, L. A.; Hill, R. M. J Chem Soc Faraday Trans II 1984, 80, 291.